

Article

Rare Earth Hydroxide as a Precursor for Controlled Fabrication of Uniform β -NaYF₄ Nanoparticles: A Novel, Low Cost, and Facile Method

Lili Xu ¹, Man Wang ¹, Qing Chen ¹, Jiajia Yang ¹, Wubin Zheng ¹, Guanglei Lv ^{1,*},
Zewei Quan ^{2,*} and Chunxia Li ^{1,*}

¹ Key Laboratory of the Ministry of Education for Advanced Catalysis Materials, Zhejiang Normal University, Jinhua 321004, China; 18329016701@163.com (L.X.); 15500100396@zjnu.edu.cn (M.W.); 1369976191@zjnu.edu.cn (Q.C.); 1547533672@zjnu.edu.cn (J.Y.); 13636130@zjnu.edu.cn (W.Z.)

² Department of Chemistry, Southern University of Science and Technology, Shenzhen 518055, China

* Correspondence: guanglei@zjnu.edu.cn (G.L.); quanzw@sustc.edu.cn (Z.Q.); cxli@zjnu.edu.cn (C.L.);
Tel.: +86-0579-82282269 (G.L. & C.L.); +86-0755-88018399 (Z.Q.)

Received: 31 December 2018; Accepted: 17 January 2019; Published: 19 January 2019



Abstract: In recent years, rare earth doped upconversion nanocrystals have been widely used in different fields owing to their unique merits. Although rare earth chlorides and trifluoroacetates are commonly used precursors for the synthesis of nanocrystals, they have certain disadvantages. For example, rare earth chlorides are expensive and rare earth trifluoroacetates produce toxic gases during the reaction. To overcome these drawbacks, we use the less expensive rare earth hydroxide as a precursor to synthesize β -NaYF₄ nanoparticles with multiform shapes and sizes. Small-sized nanocrystals (15 nm) can be obtained by precisely controlling the synthesis conditions. Compared with the previous methods, the current method is more facile and has lower cost. In addition, the defects of the nanocrystal surface are reduced through constructing core–shell structures, resulting in enhanced upconversion luminescence intensity.

Keywords: β -NaYF₄; rare earth upconversion nanoparticles; core–shell structure

1. Introduction

In recent years, Lanthanide (Ln³⁺)-doped upconversion nanoparticles (UCNPs) that convert low energy photons into high energy photons through a two- or multi-photon absorption mechanism have extensively attracted researchers' attention due to their potential applications in a variety of fields, such as bioimaging [1–8], biosensing [9,10], drug delivery [11,12], and cancer therapy [13–16]. Compared with traditional fluorescent probes, such as organic fluorescent dyes and semiconductor quantum dots, UCNPs possess some unique advantages, including weak background fluorescence, large anti-Stokes shift, high photochemical stability, narrow emission bandwidth, long luminescent lifetime, high penetration depth, and low toxicity, among others [17–24]. Among reported UCNPs, hexagonal phase (β -) sodium yttrium fluoride has been shown to be one of most efficient host materials owing to its low photon cutoff energy ($\sim 350\text{ cm}^{-1}$) and high chemical stability, which are able to effectively reduce non-radiative energy losses at the intermediate states of lanthanide ions [25]. So far, several methods have been reported to synthesize lanthanide-doped β -NaYF₄ nanoparticles with controlled crystalline phase, shape, and size. Solvothermal method and thermal decomposition methods are two of the most frequently used techniques to synthesize monodisperse lanthanide-doped β -NaYF₄ nanoparticles. For example, Haase reported the synthesis of β -NaYF₄ by using expensive rare earth chlorides as precursors [26]. Capobianco and co-workers synthesized β -NaYF₄ nanocrystals co-doped with Yb³⁺/Er³⁺ or Yb³⁺/Tm³⁺ via the thermal decomposition of rare earth trifluoroacetate

precursors where octadecene (ODE) and oleic acid (OA) were chosen as a solvent and ligand, respectively [27]. However, there are disadvantages in this method, such as the high synthetic temperature, the complicated decomposition process, and the uncontrollable experimental conditions. More importantly, the heating of trifluoroacetate would produce toxic fluorinated and oxyfluorinated carbon gases.

In this paper, we developed a novel method by using cheap rare earth hydroxide as a precursor to synthesize monodisperse hexagonal $\text{NaYF}_4:\text{Yb}^{3+}/\text{Ln}^{3+}$ core and $\text{NaYF}_4:\text{Yb}^{3+}/\text{Ln}^{3+}@\text{NaGdF}_4$ ($\text{Ln} = \text{Er}$, Tm , and Ho) core-shell nanoparticles with well-defined shapes. Compared with the previous methods, this method is low-cost and more facile. Moreover, during the reaction process no toxic gases are produced. In addition, the size of nanocrystals can be tuned by controlling the reaction conditions, such as the molar ratio of $\text{Na}^+/\text{Ln}^{3+}/\text{F}^-$, the volume ratio of OA and ODE, and the amount of sodium oleate (NaOA). Under 980 nm laser excitation, these core-shell nanoparticles showed intense upconversion emissions relative to $\text{NaYF}_4:\text{Yb}/\text{Ln}$ ($\text{Ln} = \text{Er}$, Tm , and Ho) core nanoparticles.

2. Results and Discussion

It is well known that for the synthesis of nanomaterials, sodium sources and fluorine sources are two important factors in affecting the morphology and size of nanocrystals. In our experiments, we explored the effects of sodium hydroxide (NaOH), sodium oleate (NaOA), sodium trifluoroacetate (CF_3COONa), and sodium fluoride (NaF) on the morphology and size of nanocrystals. It can be easily seen that the particle size was uneven when CF_3COONa (Figure 1A) and NaF (Figure 1B) were used as sodium sources. Moreover, their powder X-ray diffraction (XRD) patterns were in line with the standard cubic one of JCPDS 06-0342 (Figure 1E). The broader width (red pentagram) of the XRD was ascribed to the peak of silica from the slide. However, $\text{NaYF}_4:\text{Yb}^{3+}/\text{Er}^{3+}$ nanoparticles obtained with NaOH (Figure 1C) or NaOA (Figure 1D) as sodium sources had a uniform size and a crystal phase that matched well the standard JCPDS 16-0334 of $\beta\text{-NaYF}_4$ (Figure 1E). In addition, the size of the upconverting nanoparticles synthesized with NaOA was smaller than that of NaOH. This means NaOA can effectively inhibit the growth of NaYF_4 because of extra OA-ligands from NaOA. Taken together, the sodium source has a great influence on the size and crystal phase of the nanocrystals.

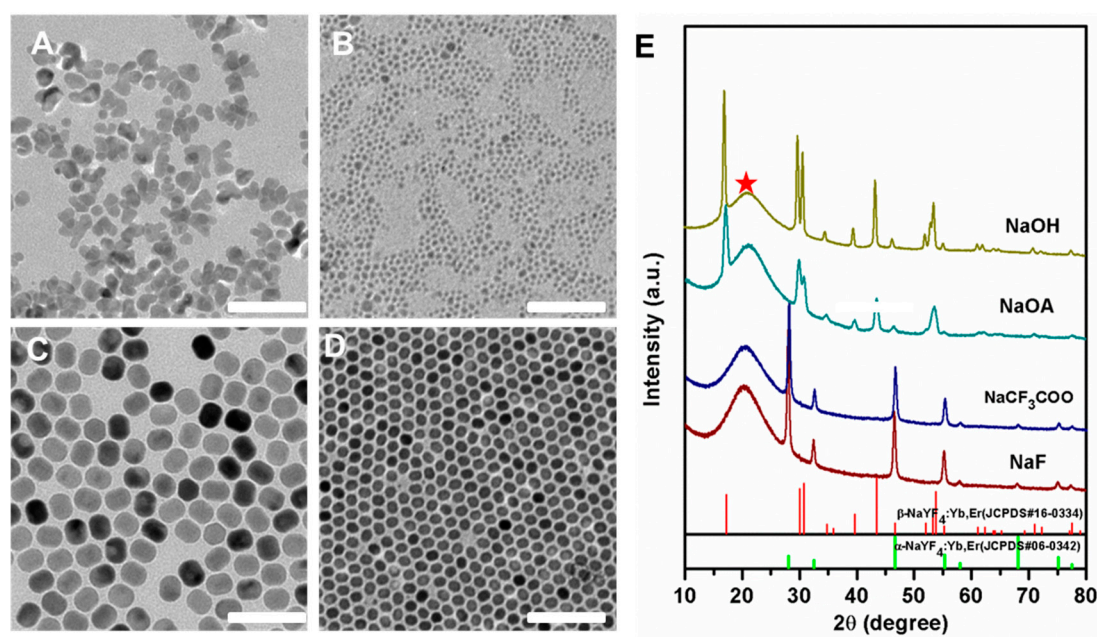


Figure 1. TEM images of $\text{NaYF}_4:\text{Yb}^{3+}/\text{Er}^{3+}$ nanocrystals synthesized with NaOH (A), NaOA (B), CF_3COONa (C), and NaF (D) as well as the corresponding XRD patterns (E). The red pentagram represents the peak of silica from the slide. The standard diffraction patterns of the $\alpha\text{-NaYF}_4$ (JCPDS 06-0342) and the $\beta\text{-NaYF}_4$ (JCPDS 16-0334) are displayed at the bottom for reference. Scale bars, 100 nm.

Based on the above results, we firstly used NaOH as sodium sources to explore the effect of $\text{Na}^+/\text{Ln}^{3+}/\text{F}^-$ on the size and morphology of nanocrystals. A series of $\text{NaYF}_4:\text{Yb}^{3+}/\text{Er}^{3+}$ nanocrystals were synthesized with different ratios of $\text{Na}^+/\text{Ln}^{3+}/\text{F}^-$ when the volume ratio of OA/ODE was fixed. Figure 2 presents the TEM images and size distributions of the $\text{NaYF}_4:\text{Yb}^{3+}/\text{Er}^{3+}$ nanocrystals. It can be clearly seen that when the molar ratio $\text{Na}^+/\text{Ln}^{3+}/\text{F}^-$ increased, the particle size of the products decreased accompanied by the shape evolution from rod to sphere. When the molar ratio of $\text{Na}^+/\text{Ln}^{3+}/\text{F}^-$ was 2.5:1:4, the nanoparticles are regular rods with good monodispersity. Their lengths and widths are 32 nm and 27 nm (Figure 2A,B and Figure S1, Supporting Information), which are obtained by randomly measuring more than 150 particles. When the ratio of $\text{Na}^+/\text{Ln}^{3+}/\text{F}^-$ was increased from 2.5:1:4 to 4:1:4, the size of the nanocrystals was reduced from 32.7 to 27.7 nm. It has been reported that the simultaneous addition of Na^+ and F^- in the solution can produce small β -phase seeds, thereby the final growth of small-sized nanocrystals can be controlled easily [28]. Moreover, the size of the nanocrystals was decreased from 25 to 23 nm when the molar ratio of $\text{Na}^+/\text{Ln}^{3+}/\text{F}^-$ was increased to be 6:1:6 (Figure 2G,H). When the molar ratio was further increased to 8:1:8 (Figure 2I,J), the size of the nanocrystals was reduced to 22 nm.

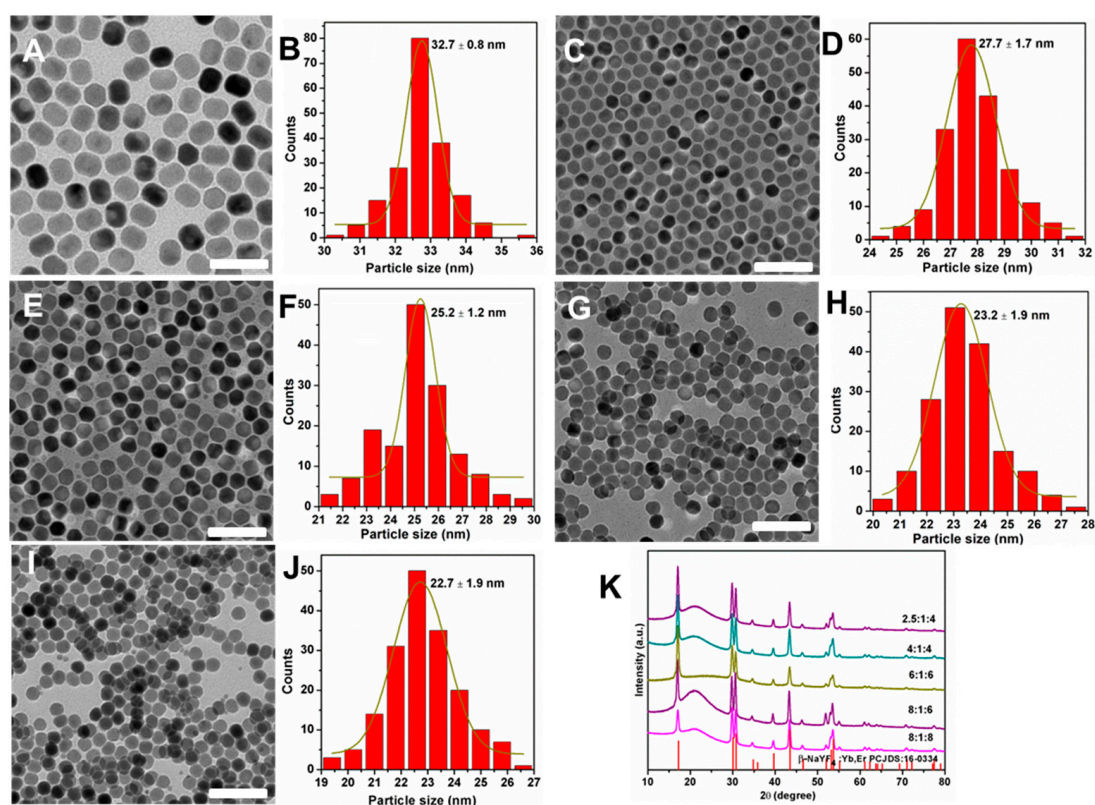


Figure 2. TEM images and size histograms of $\text{NaYF}_4:\text{Yb}^{3+}/\text{Er}^{3+}$ nanocrystals synthesized with NaOH by using $\text{Na}^+/\text{Ln}^{3+}/\text{F}^-$ with a molar ratio of 2.5:1:4 (A,B), 4:1:4 (C,D), 6:1:6 (E,F), 8:1:6 (G,H), and 8:1:8 (I,J), respectively, as well as the corresponding XRD patterns (K); the standard diffraction pattern of the β - NaYF_4 (JCPDS 16-0334) is depicted at the bottom for reference. Scale bars, 100 nm.

To clarify the role of NaOA, we further studied the effect of its amount on the synthesis of $\text{NaYF}_4:\text{Yb}^{3+}/\text{Er}^{3+}$ nanocrystals. Herein, we used NaOA substitute for NaOH to synthesize diverse nanoparticles with different molar ratios of $\text{Na}^+/\text{Ln}^{3+}/\text{F}^-$. Figure 3 shows the TEM images of as-synthesized $\text{NaYF}_4:\text{Yb}^{3+}/\text{Er}^{3+}$ nanocrystals, which exhibited the morphology and size evolution. As expected, the morphology of the nanocrystals changed from rods to spheres. Meanwhile, the size was reduced from about 24 to 16 nm. As the amount of NaOA increased from 1.5 to 2.5 mmol, the size of the nanocrystals decreased to 20 nm (Figure 3A–D). Then the size of $\text{NaYF}_4:\text{Yb}^{3+}/\text{Er}^{3+}$ nanocrystals

was further decreased to about 17 nm when the amount of NaOA increased to 6 mmol (Figure 3E,F) and 8 mmol (Figure 3G,H), respectively. It was possible that oxygen moiety in the OA–ligands had a much stronger binding affinity to Y^{3+} ions when there were adequate OA–ligands with the increased of NaOA.

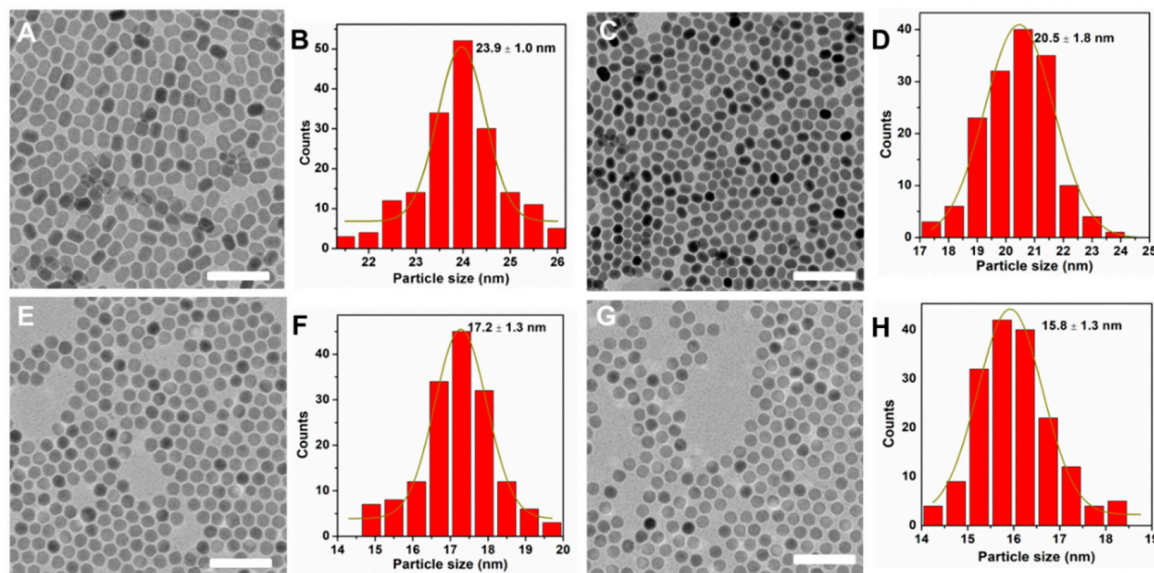


Figure 3. TEM images and size histograms of $NaYF_4:Yb^{3+}/Er^{3+}$ nanocrystals synthesized with NaOA by using $Na^+/Ln^{3+}/F^-$ with molar ratios of 1.5:1:4 (A,B), 2.5:1:4 (C,D), 6:1:4 (E,F), and 8:1:4 (G,H), respectively. Scale bars, 100 nm.

The OA–ligands can effectively induce the orderly arrangement of Y^{3+} ions during the formation process of $NaYF_4$ [29]. Additionally, when the amount of OA–ligands was adequate, they would cover the surface of the nanoparticles to inhibit the growth of nanocrystals, which is an effective method to obtain the nanocrystals with a smaller size. Figure S2 (Supporting Information) shows the XRD patterns of the as-prepared $NaYF_4:Yb^{3+}/Er^{3+}$ core nanoparticles. All the XRD patterns of samples could be matched with the pure hexagonal-phases $NaYF_4$ (JCPDS 16-0334), and no trace of other phases or impurities were observed, which clearly suggests the high crystallinities of these as-prepared nanoparticles. It has been reported that the presence of oleic acid in the solvent plays an important role in tuning the size and morphology of $NaYF_4:Yb^{3+}/Er^{3+}$ nanocrystals [30]. Figure 4 shows the TEM images and size distributions of $NaYF_4:Yb^{3+}/Er^{3+}$ nanoparticles prepared at different ratios of OA/ODE of 4/15 (Figure 4A,B), 8/15 (Figure 4C,D), 10/15 (Figure 4E,F), and 15/15 (Figure 4H,I). As can be seen, the resulting $NaYF_4:Yb^{3+}/Er^{3+}$ nanoparticles with the ratio of OA/ODE (4/15) were hexagonal in shape with an average diameter of about 26 nm. With the increased volume ratio of OA/ODE, the particle size of $NaYF_4:Yb^{3+}/Er^{3+}$ nanoparticles gradually increased, and the average diameter of nanoparticles was found to be approximately 40 nm at 8/15 of OA/ODE. The XRD of all as-prepared samples are shown in Figure S3 (Supporting Information). The same procedure was used to further synthesize $NaYF_4$ nanoparticles doped with other lanthanide elements such as 40% $Yb^{3+}/0.5\%Tm^{3+}$ (Figure S3A,B) and 18% $Yb^{3+}/2\%Ho^{3+}$ (Figure S3C,D, Supporting Information), respectively. It was observed that the size and morphology of the nanoparticles closely resembled those of the Yb^{3+}/Er^{3+} co-doped $NaYF_4$ counterpart (Figure S1, Supporting Information). These results indicate that the change of dopant ions in low doping concentrations does not alter the particle growth process [31].

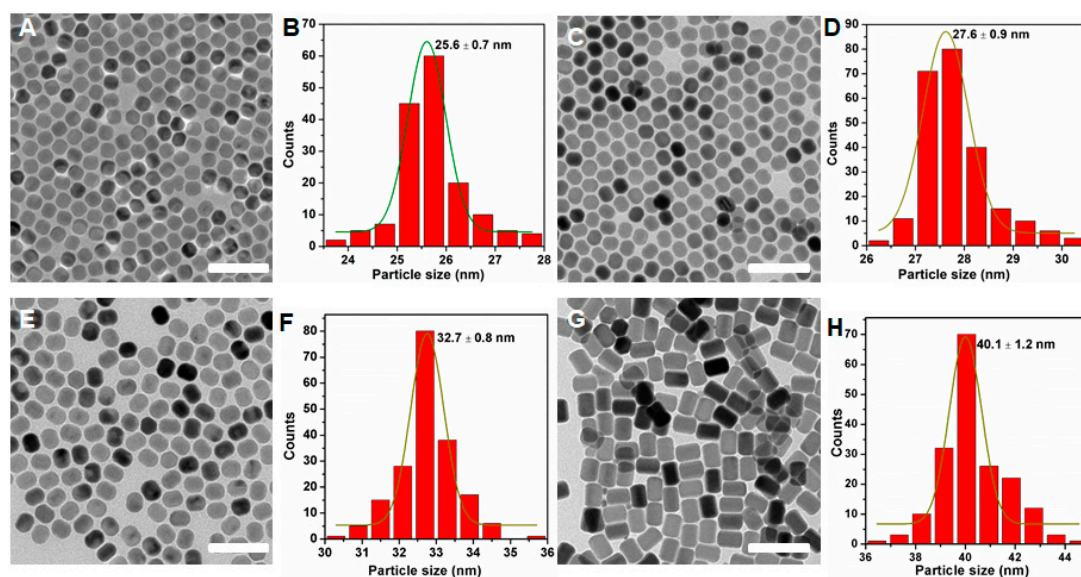


Figure 4. TEM images and size histograms of $\text{NaYF}_4:\text{Yb}^{3+}/\text{Er}^{3+}$ nanocrystals synthesized at varied amounts of oleic acid (OA). The volume ratios of OA and octadecene (ODE) are 4:15 (A,B), 8:15 (C,D), 10:15 (E,F), and 15:15 (G,H), respectively. Scale bars, 100 nm.

More importantly, the emission intensity of Ln^{3+} doped UCNP depends on dopant–host combination, particle size, shape, and phase [32–38]. The emission intensity of NaYF_4 core was relatively weak due to the surface defects. However, in recent years, the construction of core–shell structure has been one of the effective ways to improve the efficiency of upconversion luminescence [26,39–42]. This is because the inert shell coating can protect the luminescent activators in the core nanoparticles from the surface quenching of excitation energy [42]. In this paper, we prepared $\text{NaYF}_4:\text{Yb}^{3+}/\text{Ln}^{3+}@\text{NaGdF}_4$ and studied their upconversion optical properties. Figure 5A–F displays the TEM images and the corresponding size distribution of $\text{NaYF}_4:\text{Yb}^{3+}/\text{Ln}^{3+}@\text{NaGdF}_4$ core–shell nanoparticles. The $\text{NaYF}_4:\text{Yb}^{3+}/\text{Er}^{3+}$ core-only nanoparticles with an average diameter of about 27 nm are shown in Figure S1. After coating an inert shell layer of NaGdF_4 , the average diameter of $\text{NaYF}_4:\text{Yb}^{3+}/\text{Er}^{3+}@\text{NaGdF}_4$ core–shell was determined to be about 42 nm, which means a thick shell layer (thickness ~ 7.5 nm) was coated around the $\text{NaYF}_4:\text{Yb}^{3+}/\text{Er}^{3+}$ core nanoparticles (Figure 5A,B). Similar TEM image and size distribution were obtained for $\text{NaYF}_4:\text{Yb}^{3+}/\text{Tm}^{3+}@\text{NaGdF}_4$ (Figure 5C,D) and $\text{NaYF}_4:\text{Yb}^{3+}/\text{Ho}^{3+}@\text{NaGdF}_4$ (Figure 5E,F) core–shell nanoparticles. The corresponding shell thickness was determined to be about 11 nm and 9 nm, respectively. Figure 5G depicts the upconversion emission spectra for the $\text{NaYF}_4:\text{Yb}^{3+}/\text{Er}^{3+}$ core nanoparticles and the $\text{NaYF}_4:\text{Yb}^{3+}/\text{Er}^{3+}@\text{NaGdF}_4$ core–shell nanoparticles. As can be seen, there were two green emission bands centered at 520 nm and 540 nm, which were attributed to the electronic transition of ${}^2\text{H}_{11/2} \rightarrow {}^4\text{I}_{15/2}$, ${}^4\text{S}_{3/2} \rightarrow {}^4\text{I}_{15/2}$ of Er^{3+} . In addition, there was a red emission at 654 nm, which corresponded to the ${}^4\text{F}_{9/2} \rightarrow {}^4\text{I}_{15/2}$ transition of Er^{3+} . For the $\text{NaYF}_4:\text{Yb}^{3+}/\text{Er}^{3+}$ core, after coating 7.5 nm NaGdF_4 shell, the fluorescence intensity of $\text{NaYF}_4:\text{Yb}^{3+}/\text{Er}^{3+}@\text{NaGdF}_4$ core–shell nanoparticles was about 100 times higher than that of $\text{NaYF}_4:\text{Yb}^{3+}/\text{Er}^{3+}$ core nanoparticles at 540 nm. In contrast, for the $\text{NaYF}_4:\text{Yb}^{3+}/\text{Tm}^{3+}$ core nanoparticles, the blue emissions, the ultraviolet emission, and red emission corresponded to the (${}^1\text{I}_6 \rightarrow {}^3\text{F}_4$, 342 nm, ${}^1\text{D}_2 \rightarrow {}^3\text{H}_6$, 360 nm), (${}^1\text{D}_2 \rightarrow {}^3\text{F}_4$, 450 nm, ${}^1\text{G}_4 \rightarrow {}^3\text{H}_6$, 475 nm), (${}^1\text{G}_4 \rightarrow {}^3\text{F}_4$, 647 nm) transitions of Tm^{3+} ions, respectively. Due to the NaGdF_4 (~ 11 nm) shell coating, the emission intensity was remarkably enhanced to about 120 times at 475 nm (Figure 5G). Figure 5H shows the upconversion emission spectra of the $\text{NaYF}_4:\text{Yb}^{3+}/\text{Ho}^{3+}$ core nanoparticles and the $\text{NaYF}_4:\text{Yb}^{3+}/\text{Ho}^{3+}@\text{NaGdF}_4$ core–shell nanoparticles. When excited at 980 nm, three upconversion fluorescence bands with maxima at green (540 nm), red (645 nm), and 750 nm regions could be observed from optimized $\text{NaYF}_4:\text{Yb}^{3+}/\text{Ho}^{3+}$ nanophosphors, which corresponded to ${}^5\text{S}_2 \rightarrow {}^5\text{I}_8$, ${}^5\text{F}_3 \rightarrow {}^5\text{I}_8$, and ${}^5\text{S}_2 \rightarrow {}^5\text{I}_7$ transitions of Ho^{3+} ions. Similarly, when the ~ 9 nm NaGdF_4 shell was covered on the surface

of the $\text{NaYF}_4:\text{Yb}^{3+}/\text{Ho}^{3+}$ core, the luminescence intensity was also significantly improved. The emission intensity of $\text{NaYF}_4:\text{Yb}^{3+}/\text{Ho}^{3+}@\text{NaGdF}_4$ core-shell nanoparticles was determined to be about 80 times as strong as that of $\text{NaYF}_4:\text{Yb}^{3+}/\text{Ho}^{3+}$ core nanoparticles.

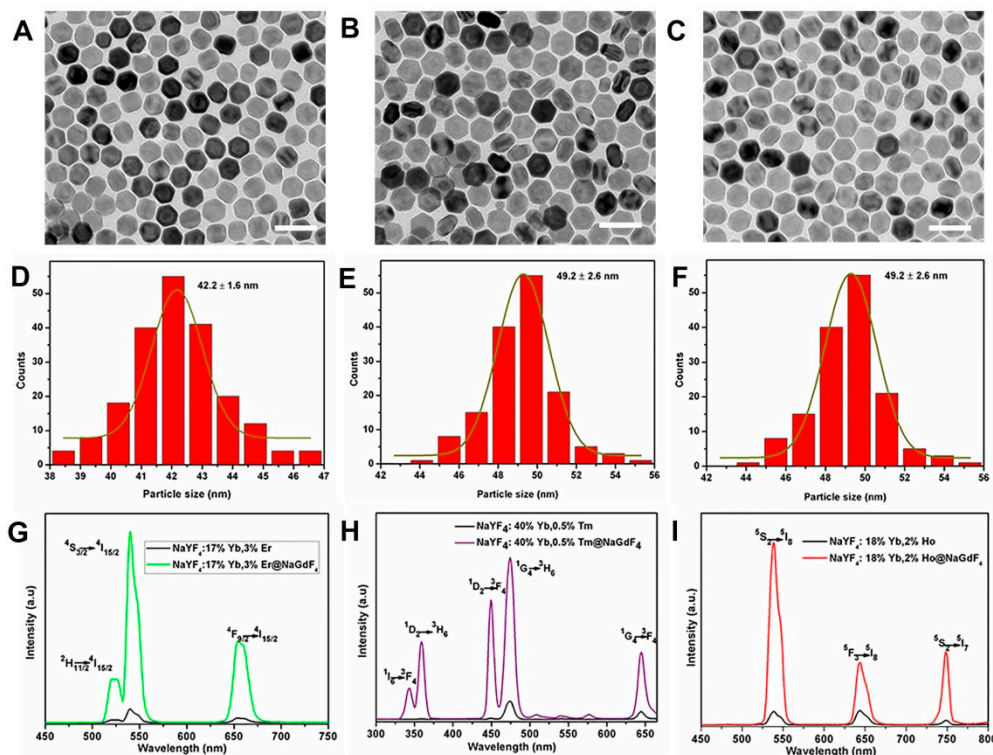


Figure 5. TEM images, size histograms, and the corresponding upconversion spectra of core-shell structured $\text{NaYF}_4:\text{Yb}^{3+}/\text{Er}^{3+}@\text{NaGdF}_4$ (A,D,G), $\text{NaYF}_4:\text{Yb}^{3+}/\text{Tm}^{3+}@\text{NaGdF}_4$ (B,E,H), and $\text{NaYF}_4:\text{Yb}^{3+}/\text{Ho}^{3+}@\text{NaGdF}_4$ (C,F,I), respectively. Scale bars, 100 nm.

3. Materials and Methods

3.1. Materials

Materials Y_2O_3 (99.99%), Yb_2O_3 (99.99%), Er_2O_3 (99.99%), Tm_2O_3 (99.99%), Ho_2O_3 (99.99%), Y_2O_3 (99.99%), $\text{GdCl}_3 \cdot 6\text{H}_2\text{O}$ (99.99%), NH_4F (98%), NaF (98%), and CF_3COONa (97%) were purchased from Aladdin (Shanghai, China). Oleic acid (OA, 90%), 1-octadecene (ODE, 90%), and sodium oleate (Na-OA, >97%) were purchased from Sigma-Aldrich (Darmstadt, Germany). Other chemical reagents, such as NaOH (90%), ethyl alcohol (99.7%), methanol (99.5%), and *n*-hexane (97%), were obtained from Shanghai Lingfeng Chemical Reagent Co., Ltd. All chemicals were used as received without further purification.

Rare earth chloride (LnCl_3) stock solutions of 1 M ($\text{Ln} = \text{Y}, \text{Yb}$) and 0.1 M ($\text{Ln} = \text{Er}, \text{Tm}, \text{and Ho}$) were prepared by dissolving the corresponding metal oxides in hydrochloric acid at elevated temperature. The final solutions were adjusted to pH ~6.

3.2. Synthesis of $\beta\text{-NaYF}_4:\text{Yb}^{3+}/\text{Ln}^{3+}$ ($\text{Ln} = \text{Er}, \text{Tm}$ and Ho) Core Nanoparticles

First, $\text{Ln}(\text{OH})_3$ ($\text{Ln} = \text{Y}^{3+}, \text{Yb}^{3+}, \text{and Er}^{3+}/\text{Tm}^{3+}/\text{Ho}^{3+}$) complexes were prepared by adding NaOH of 2 M to the rare earth chloride solution, and then the obtained product was washed twice. Rare earth hydroxide was added to a 100 mL flask containing 10 mL of OA and 15 mL of ODE. The mixture was heated at 140 °C for 1 h under stirring in order to form the lanthanide-oleate complexes. After cooling down to 40 °C naturally, 8 mL of methanol solution containing NH_4F (4 mmol) and NaOH (2.5 mmol) was added. Subsequently, the resulting mixture solution was heated at 70 °C for 10 min to evaporate

the methanol under magnetic stirring. After the temperature was raised up to 110 °C under vacuum for 30 min, the reaction mixture was heated to 300 °C under argon for 1 h and then cooled down to room temperature. The resulting nanoparticles were precipitated by adding excess ethanol, separated by centrifugation at 4000 rpm for 4 min, washed with a mixture of *n*-hexane and ethanol several times, and finally dispersed in *n*-hexane for further use.

3.3. Synthesis of β -NaYF₄:Yb/Ln@NaGdF₄ (Ln = Er, Tm, and Ho) Core–Shell Nanoparticles

In a typical procedure for the synthesis of NaYF₄:Yb³⁺/Er³⁺ (17/3%)@NaGdF₄ nanoparticles, the NaGdF₄ inert shell precursor was prepared by mixing 0.5 mmol of GdCl₃ with 6 mL of OA and 15 mL of ODE in a 100 mL flask followed by heating at 150 °C for 40 min. Then, the obtained NaGdF₄ inert shell precursor was cooled down to room temperature. Subsequently, the NaYF₄:Yb³⁺/Er³⁺ (17/3%) core-only nanoparticles dispersed in 3 mL of cyclohexane along with 8 mL of methanol solution of NH₄F (2 mmol) and NaOH (1.25 mmol) was added. Subsequently, the resulting mixture solution was heated at 70 °C for 10 min under magnetic stirring to evaporate the methanol. After the resulting solution for 30 min at 110 °C under vacuum, the reaction mixture was heated to 310 °C under argon for 1.5 h and then cooled down to room temperature. Finally, the obtained core–shell nanoparticle products were precipitated by the addition of ethanol, collected by centrifugation at 4000 rpm for 4 min, washed with a mixture of *n*-hexane and ethanol several times, and finally dispersed in *n*-hexane.

3.4. Instrumentation

Transmission electron microscopy (TEM) images (Hitachi, Tokyo, Japan) were acquired on a HT7700 transmission electron microscopy at an acceleration voltage of 100 kV. X-ray diffraction (XRD) patterns were recorded on an X-ray diffraction (RigakuSmartLab, Tokyo, Japan) with Cu K α radiation ($\lambda = 0.15418$ nm) at a voltage of 45 kV and a current of 20 mA. Upconversion luminescence spectra were detected by a spectrophotometer (FluoroMax-4, Shanghai, China) equipped with a 980 nm diode laser.

4. Conclusions

In summary, we developed a novel, facile, and low-cost method to synthesize Yb³⁺/Ln³⁺ (Ln = Er, Tm, and Ho) co-doped β -NaYF₄ nanocrystals. The size and morphology of the products were manipulated through the precise tuning of the ratio of Na⁺/Ln³⁺/F[−], the ratio of OA/ODE, and the quantity of the NaOA. As the ratio of Na⁺/Ln³⁺/F[−] and the amount of NaOA increased, the size of the nanocrystals gradually decreased and the corresponding morphologies evolved from nanospheres to nanorods. Finally, this method can also apply to the fabrication of core–shell structured nanomaterials. The uniform NaYF₄:Yb³⁺/Ln³⁺@NaGdF₄ core–shell nanoparticles were prepared successfully, and their emission intensity was remarkably enhanced, which could provide prospect applications in the biomedical fields. Particularly, some photosensitizers or chemotherapy drugs could be conjugated with these UCNPs to achieve NIR-triggered drug delivery and controlled release to ameliorate the therapy efficiency of tumors.

Supplementary Materials: The following are available online, Figure S1: TEM image (A) and the corresponding size histogram (B) of NaYF₄:Yb³⁺/Er³⁺ nanocrystals synthesized with NaOH as sodium source, Figure S2: XRD patterns of the as-synthesized NaYF₄:Yb³⁺/Er³⁺ nanocrystals with NaOA at varied molar ratios of Na⁺/Ln³⁺/F[−]. The standard diffraction patterns of the β -NaYF₄ (JCPDS 16-0334) depicted at the bottom for reference, Figure S3: XRD patterns of the as-synthesized NaYF₄:Yb³⁺/Er³⁺ nanocrystals at varied amounts of oleic acid. The volume ratios of oleic acid and octadecene are 15:15, 10:15, 8:15, and 4:15, respectively. The diffraction pattern at the bottom is the literature reference for hexagonal NaYF₄ nanocrystal (JCPDS 16-0334), Figure S4: TEM images and size histograms of the NaYF₄:Yb³⁺/Er³⁺ (A, B), and NaYF₄:Yb³⁺/Ho³⁺ (C, D), respectively.

Author Contributions: Conceptualization, L.X. and G.L.; investigation and data curation, M.W. and Q.C.; writing and original draft preparation, L.X. and J.Y.; writing, reviewing, and editing, W.Z., C.L. and G.L.; and supervision, G.L., Z.Q. and C.L.

Funding: This research was funded by the National Natural Science Foundation of China (51572258, 51872263 and 51772142), Zhejiang Provincial Natural Science Foundation of China (LZ19E020001 and LQ19B050003), the Key Construction Project (2017XM022) of Zhejiang Normal University and Open Research Fund of Key Laboratory of the Ministry of Education for Advanced Catalysis Materials, and Zhejiang Key Laboratory for Reactive Chemistry on Solid Surfaces, Zhejiang Normal University.

Conflicts of Interest: The authors declare no conflict of interest.

References

1. Park, I.; Lee, K.T.; Suh, Y.D.; Hyeon, T. Upconverting nanoparticles: A versatile platform for wide-field two-photon microscopy and multi-modal in vivo imaging. *Chem. Soc. Rev.* **2015**, *44*, 1302–1317. [[CrossRef](#)] [[PubMed](#)]
2. Dong, H.; Sun, L.D.; Wang, Y.F.; Ke, J.; Si, R.; Xiao, J.W.; Lyu, G.M.; Shi, S.; Yan, C.H. Efficient Tailoring of Upconversion Selectivity by Engineering Local Structure of Lanthanides in $\text{Na}_x\text{REF}_{3+x}$ Nanocrystals. *J. Am. Chem. Soc.* **2015**, *137*, 6569–6576. [[CrossRef](#)] [[PubMed](#)]
3. Wolfbeis, O.S. An overview of nanoparticles commonly used in fluorescent bioimaging. *Chem. Soc. Rev.* **2015**, *44*, 4743–4768. [[CrossRef](#)]
4. Wei, Z.W.; Sun, L.N.; Liu, J.L.; Zhang, J.Z.; Yang, H.R.; Yang, Y.; Shi, L.Y. Cysteine modified rare-earth up-converting nanoparticles for in vitro and in vivo bioimaging. *Biomaterials* **2014**, *35*, 387–392. [[CrossRef](#)] [[PubMed](#)]
5. Zhang, H.; Wu, Y.; Wang, J.; Tang, Z.M.; Ren, Y.; Ni, D.L.; Gao, H.B.; Song, R.X.; Jin, T.; Li, Q.; et al. In Vivo MR Imaging of Glioma Recruitment of Adoptive T-Cells Labeled with NaGdF_4 -TAT Nanoprobes. *Small* **2017**, *14*, 1702951–1702959. [[CrossRef](#)] [[PubMed](#)]
6. Deng, M.L.; Wang, L.Y. Unexpected luminescence enhancement of upconverting nanocrystals by cation exchange with well retained small particle size. *Nano Res.* **2014**, *7*, 782–793. [[CrossRef](#)]
7. Xu, S.; Yu, Y.; Gao, Y.F.; Zhang, Y.Q.; Li, X.P.; Zhang, J.S.; Wang, Y.F.; Chen, B.J. Mesoporous silica coating $\text{NaYF}_4:\text{Yb,Er}@/\text{NaYF}_4$ upconversion nanoparticles loaded with ruthenium(II) complex nanoparticles: Fluorometric sensing and cellular imaging of temperature by upconversion and of oxygen by downconversion. *Microchim. Acta* **2018**, *185*, 454–463. [[CrossRef](#)] [[PubMed](#)]
8. Lei, X.L.; Li, R.F.; Tu, D.T.; Shang, X.Y.; Liu, Y.; You, W.W.; Sun, C.X.; Zhang, F.; Chen, X.Y. Intense near-infrared-II luminescence from $\text{NaCeF}_4:\text{Er}/\text{Yb}$ nanoprobes for in vitro bioassay and in vivo bioimaging. *Chem. Sci.* **2018**, *9*, 4682–4988. [[CrossRef](#)] [[PubMed](#)]
9. Liu, J.; Liu, Y.; Bu, W.; Bu, J.; Sun, Y.; Du, J.; Shi, J. Ultrasensitive Nanosensors Based on Upconversion Nanoparticles for Selective Hypoxia Imaging in vivo upon Near-Infrared Excitation. *J. Am. Chem. Soc.* **2014**, *136*, 9701–9709. [[CrossRef](#)] [[PubMed](#)]
10. Zheng, W.; Tu, D.T.; Huang, P.; Zhou, S.Y.; Chen, Z.; Chen, X.Y. Time-resolved luminescent biosensing based on inorganic lanthanide-doped nanoprobes. *Chem. Commun.* **2015**, *51*, 4129–4143. [[CrossRef](#)] [[PubMed](#)]
11. Jalani, G.; Tam, V.; Vetrone, F.; Cerruti, M. Seeing, Targeting and Delivering with Upconverting Nanoparticles. *J. Am. Chem. Soc.* **2018**, *140*, 10923–10931. [[CrossRef](#)] [[PubMed](#)]
12. Zhang, Y.; Yu, Z.Z.; Li, J.Q.; Ao, Y.X.; Xue, J.W.; Zeng, Z.P.; Yang, X.L.; Tan, T.T.Y. Ultrasmall-Superbright Neodymium-Upconversion Nanoparticles via Energy Migration Manipulation and Lattice Modification: 808 nm-Activated Drug Release. *ACS Nano* **2017**, *11*, 2846–2857. [[CrossRef](#)] [[PubMed](#)]
13. Zhang, C.; Chen, W.H.; Liu, L.H.; Qiu, W.X.; Yu, W.Y.; Zhang, X.Z. An O_2 Self-Supplementing and Reactive-Oxygen-Species-Circulating Amplified Nanoplatform via $\text{H}_2\text{O}/\text{H}_2\text{O}_2$ Splitting for Tumor Imaging and Photodynamic Therapy. *Adv. Funct. Mater.* **2017**, *27*, 1700626–1700639. [[CrossRef](#)]
14. Lu, S.; Tu, D.T.; Hu, P.; Xu, J.; Li, R.F.; Wang, M.; Chen, Z.; Huang, M.D.; Chen, X.Y. Multifunctional Nano-Bioprobes Based on Rattle-Structured Upconverting Luminescent Nanoparticles. *Angew. Chem. Int. Ed.* **2015**, *54*, 7915–7919. [[CrossRef](#)] [[PubMed](#)]
15. Zhu, X.J.; Li, J.C.; Qiu, X.C.; Liu, Y.; Wang, F.; Li, F.Y. Upconversion nanocomposite for programming combination cancer therapy by precise control of microscopic temperature. *Nat. Commun.* **2018**, *9*, 2176–2186. [[CrossRef](#)] [[PubMed](#)]
16. Zhang, C.; Zhao, K.L.; Bu, W.B.; Ni, D.L.; Liu, Y.Y.; Feng, J.W.; Shi, J.L. Marriage of Scintillator and Semiconductor for Synchronous Radiotherapy and Deep Photodynamic Therapy with Diminished Oxygen Dependence. *Angew. Chem. Int. Ed.* **2015**, *54*, 1770–1774. [[CrossRef](#)]

17. Yang, D.M.; Ma, P.A.; Hou, Z.Y.; Cheng, Z.Y.; Li, C.X.; Lin, J. Current advances in lanthanide ion (Ln^{3+})-based upconversion nanomaterials for drug delivery. *Chem. Soc. Rev.* **2015**, *44*, 1416–1448. [[CrossRef](#)]
18. Liu, Y.S.; Tu, D.T.; Zhu, H.M.; Chen, X.Y. Photon upconversion nanomaterials. *Chem. Soc. Rev.* **2015**, *44*, 1299–1301. [[CrossRef](#)]
19. Zeng, S.J.; Wang, H.B.; Lu, W.; Yi, Z.G.; Rao, L.; Liu, H.R.; Hao, J.H. Dual-modal upconversion fluorescent/X-ray imaging using ligand-free hexagonal phase $\text{NaLuF}_4:\text{Gd}/\text{Yb}/\text{Er}$ nanorods for blood vessel visualization. *Biomaterials* **2014**, *35*, 2934–2941. [[CrossRef](#)]
20. Wang, C.; Yao, W.X.; Wang, P.Y.; Zhao, M.Y.; Li, X.M.; Zhang, F. A catalase-loaded hierarchical zeolite as an implantable nanocapsule for ultrasound-guided oxygen self-sufficient photodynamic therapy against pancreatic cancer. *Adv. Mater.* **2018**, *30*, 1704833–1704840.
21. Chen, D.Q.; Chen, Y.; Lu, H.W.; Ji, Z.G. A Bifunctional $\text{Cr}/\text{Yb}/\text{Tm}:\text{Ca}_3\text{Ga}_2\text{Ge}_3\text{O}_{12}$ Phosphor with Near-Infrared Long-Lasting Phosphorescence and Upconversion Luminescence. *Inorg. Chem.* **2014**, *53*, 8638–8645. [[CrossRef](#)] [[PubMed](#)]
22. Shi, Z.L.; Duan, Y.; Zhu, X.J.; Wang, Q.W.; Li, D.D.; Hu, K.; Feng, W.; Li, F.Y.; Xu, C.X. Dual functional $\text{NaYF}_4:\text{Yb}^{3+}, \text{Er}^{3+}@\text{NaYF}_4:\text{Yb}^{3+}, \text{Nd}^{3+}$ core-shell nanoparticles for cell temperature sensing and imaging. *Nanotechnology* **2018**, *29*, 094001–094009. [[CrossRef](#)] [[PubMed](#)]
23. Dai, Y.L.; Xiao, H.H.; Liu, J.H.; Yuan, Q.H.; Ma, P.A.; Yang, D.M.; Li, C.X.; Cheng, Z.Y.; Hou, Z.Y.; Yang, P.P.; et al. In vivo multimodality imaging and cancer therapy by near-infrared light-triggered trans-platinum pro-drug-conjugated upconversion nanoparticles. *J. Am. Chem. Soc.* **2013**, *135*, 18920–18929. [[CrossRef](#)] [[PubMed](#)]
24. Yu, Z.S.; Xia, Y.Z.; Xing, J.; Li, Z.H.; Zhen, J.J.; Jin, Y.H.; Tian, Y.C.; Liu, C.; Jiang, Z.Q.; Li, J.; Wu, A.G. Y1-receptor-ligand-functionalized ultrasmall upconversion nanoparticles for tumortargeted trimodality imaging and photodynamic therapy with low toxicity. *Nanoscale* **2018**, *10*, 17038–17052. [[CrossRef](#)] [[PubMed](#)]
25. Wang, F.; Liu, X.G. Recent advances in the chemistry of lanthanide-doped upconversion nanocrystals. *Chem. Soc. Rev.* **2009**, *38*, 976–989. [[CrossRef](#)] [[PubMed](#)]
26. Homann, C.; Krukewitt, L.; Frenzel, F.; Grauel, B.; Wgrth, C.; Resch-Genger, U.; Haase, M. $\text{NaYF}_4:\text{Yb}, \text{Er}/\text{NaYF}_4$ Core/Shell Nanocrystals with High Upconversion Luminescence Quantum Yield. *Angew. Chem. Int. Ed.* **2018**, *57*, 8765–8769. [[CrossRef](#)]
27. Boyer, J.C.; Vetrone, F.; Cuccia, L.A.; Capobianco, J.A. Synthesis of colloidal upconverting NaYF_4 nanocrystals doped with Er^{3+} , Yb^{3+} and Tm^{3+} , Yb^{3+} via thermal decomposition of lanthanide trifluoroacetate precursors. *J. Am. Chem. Soc.* **2006**, *128*, 7444–7445. [[CrossRef](#)]
28. Li, H.; Xu, L.; Chen, G.Y. Controlled Synthesis of Monodisperse Hexagonal $\text{NaYF}_4:\text{Yb}/\text{Er}$ Nanocrystals with Ultrasmall Size and Enhanced Upconversion Luminescence. *Molecules* **2017**, *22*, 2113. [[CrossRef](#)]
29. Liu, D.M.; Xu, X.X.; Du, Y.; Qin, X.; Zhang, Y.H.; Ma, C.S.; Wen, S.H.; Ren, W.; Goldys, E.M.; Piper, J.A.; et al. Three-dimensional controlled growth of monodisperse sub-50 nm heterogeneous nanocrystals. *Nat. Commun.* **2016**, *7*, 10254–10261. [[CrossRef](#)]
30. Huang, X.Y. Synthesis, multicolour tuning, and emission enhancement of ultrasmall $\text{LaF}_3:\text{Yb}^{3+}/\text{Ln}^{3+}$ ($\text{Ln} = \text{Er}, \text{Tm}, \text{and Ho}$) upconversion nanoparticles. *J. Mater. Sci.* **2016**, *51*, 3490–3499. [[CrossRef](#)]
31. Chen, G.Y.; Ågren, H.; Ohulchanskyy, T.Y.; Prasad, P.N. Light upconverting core-shell nanostructures: Nanophotonic control for emerging applications. *Chem. Soc. Rev.* **2015**, *44*, 1680–1713. [[CrossRef](#)] [[PubMed](#)]
32. Han, S.Y.; Deng, R.R.; Xie, X.J.; Liu, X.G. Enhancing Luminescence in Lanthanide-Doped Upconversion Nanoparticles. *Angew. Chem. Int. Ed.* **2014**, *53*, 11702–11715. [[CrossRef](#)] [[PubMed](#)]
33. Wang, F.; Han, Y.; Lim, C.S.; Lu, Y.H.; Wang, J.; Xu, J.; Chen, H.Y.; Zhang, C.; Hong, M.H.; Liu, X.G. Simultaneous phase and size control of upconversion nanocrystals through lanthanide doping. *Nature* **2010**, *463*, 1061–1065. [[CrossRef](#)] [[PubMed](#)]
34. Chen, X.; Jin, L.M.; Kong, W.; Sun, T.Y.; Zhang, W.F.; Liu, X.H.; Fan, J.; Yu, S.F.; Wang, F. Confining energy migration in upconversion nanoparticles towards deep ultraviolet lasing. *Nat. Commun.* **2016**, *7*, 10304–10309. [[CrossRef](#)] [[PubMed](#)]
35. Das, A.; Mao, C.; Cho, S.; Kim, K.; Park, W. Over 1000-fold enhancement of upconversion luminescence using water-dispersible metalinsulator-metal nanostructures. *Nat. Commun.* **2018**, *9*, 4828–4839. [[CrossRef](#)] [[PubMed](#)]
36. Cheng, T.; Marin, R.; Skripka, A.; Vetrone, F. Small and Bright Lithium-Based Upconverting Nanoparticles. *J. Am. Chem. Soc.* **2018**, *140*, 12890–12899. [[CrossRef](#)]

37. Moon, B.S.; Kim, H.E.; Kim, D.H. Ultrafast Single-Band Upconversion Luminescence in a Liquid-Quenched Amorphous Matrix. *Adv. Mater.* **2018**, *30*, 1800008. [[CrossRef](#)]
38. Cheng, X.W.; Pan, Y.; Yuan, Z.; Wang, X.W.; Su, W.H.; Yin, L.S.; Xie, X.J.; Huang, L. Er³⁺ Sensitized Photon Upconversion Nanocrystals. *Adv. Funct. Mater.* **2018**, *28*, 1800208–1800213. [[CrossRef](#)]
39. Xia, M.; Zhou, D.C.; Yang, Y.; Yang, Z.W.; Qiu, J.B. Synthesis of Ultrasmall Hexagonal NaGdF₄:Yb³⁺Er³⁺@NaGdF₄:Yb³⁺@NaGdF₄:Nd³⁺ Active-Core/Active-Shell/Active-Shell Nanoparticles with Enhanced Upconversion Luminescence. *ECS J. Solid State Sci. Technol.* **2017**, *6*, R41–R46. [[CrossRef](#)]
40. Yi, G.S.; Chow, G.M. Water-soluble NaYF₄:Yb, Er(Tm)/NaYF₄/polymer core/shell/shell Nanoparticles with Significant Enhancement of Upconversion Fluorescence. *Chem. Mater.* **2007**, *19*, 341–343. [[CrossRef](#)]
41. Shi, R.K.; Ling, X.C.; Li, X.N.; Zhang, L.; Lu, M.; Xie, X.J.; Huang, L.; Huang, W. Tuning hexagonal NaYbF₄ nanocrystals down to sub-10 nm for enhanced photon upconversion. *Nanoscale* **2017**, *9*, 13739–13746. [[CrossRef](#)] [[PubMed](#)]
42. Liu, Y.; Tu, D.; Zhu, H.; Chen, X. Lanthanide-doped luminescent nanoprobes: Controlled synthesis, optical spectroscopy, and bioapplications. *Chem. Soc. Rev.* **2013**, *42*, 6924–6958. [[CrossRef](#)] [[PubMed](#)]

Sample Availability: Not available.



© 2019 by the authors. Licensee MDPI, Basel, Switzerland. This article is an open access article distributed under the terms and conditions of the Creative Commons Attribution (CC BY) license (<http://creativecommons.org/licenses/by/4.0/>).